

Document Version

Final published version

Licence

CC BY-NC-ND

Citation (APA)

Martin, H. A., Zhang, Z., Saeed, M., Dorrestein, S., Smits, E. C. P., Poelma, R. H., van Driel, W. D., & Zhang, G. Q. (2026). Co-packaged electronics with microfluidics for direct-to-package cooling. *Communications Engineering*, 5(1), Article 92. <https://doi.org/10.1038/s44172-026-00620-9>

Important note

To cite this publication, please use the final published version (if applicable).
Please check the document version above.

Copyright

In case the licence states "Dutch Copyright Act (Article 25fa)", this publication was made available Green Open Access via the TU Delft Institutional Repository pursuant to Dutch Copyright Act (Article 25fa, the Taverne amendment). This provision does not affect copyright ownership.
Unless copyright is transferred by contract or statute, it remains with the copyright holder.

Sharing and reuse

Other than for strictly personal use, it is not permitted to download, forward or distribute the text or part of it, without the consent of the author(s) and/or copyright holder(s), unless the work is under an open content license such as Creative Commons.

Takedown policy

Please contact us and provide details if you believe this document breaches copyrights.
We will remove access to the work immediately and investigate your claim.

<https://doi.org/10.1038/s44172-026-00620-9>

Co-packaged electronics with microfluidics for direct-to-package cooling

Check for updates

Henry A. Martin^{1,2,3} , Zihan Zhang³, Mahad Saeed^{1,4}, Sander Dorrestein^{1,2}, Edsger C. P. Smits^{1,2}, René H. Poelma^{3,5}, Willem D. van Driel³ & GuoQi Zhang³

Power semiconductors operating under high heat fluxes and elevated temperatures rely on liquid-cooled heat sinks with substantial coolant volumes. Recent advancements in direct-to-chip (D2C) cooling techniques have shown enhanced thermal performance, reduced energy consumption, compact form factor, and minimized coolant usage. However, integrating microchannels onto semiconductor substrates poses significant fabrication challenges. Hence, we propose a direct-to-package (D2P) cooling approach that embeds microchannels within the package substrate, thereby bypassing the need for Thermal Interface Materials and complex fabrication processes. This D2P approach achieves high heat flux dissipation (up to $\sim 625 \text{ W cm}^{-2}$) tested in this study, while consuming a fraction of the coolant volume ($\sim 2 - 4 \text{ mL}$). The co-packaged architecture demonstrates $\sim 6 - 7 \times$ lower junction temperatures and thermal resistances than ambient-air cooling and $\sim 2 - 3 \times$ lower than heat sink cooling. A very high coefficient of performance is achieved, with an effective global Nusselt number > 10 . This work establishes D2P liquid cooling integration as a scalable and energy-efficient approach for high-power systems.

The drive towards miniaturization and increasing power densities exacerbates thermal management challenges in discrete power semiconductor devices. Power inverters in electric vehicles (EV) experience temperature fluctuations exceeding $> 110 \text{ }^\circ\text{C}$, with heat flux ranging from $\sim 100 \text{ W cm}^{-2}$ to $\sim 1000 \text{ W cm}^{-2}$, respectively^{1,2}.

Consequently, traditional cooling methods based on free and forced air convection are thermally limited due to their low convective heat transfer coefficients compared to those of liquids and steam under forced convection (see Table 1). Up to $\sim 55\%$ failures in power converters are associated with thermal stresses³, and prolonged exposure to elevated temperatures reduces the device lifespan and compromises the system efficiency and performance. Hence, there is a strong demand for innovative thermal management approaches, which is reflected in the global market for thermal management technologies, projected to reach USD 8.9 billion in 2024⁴.

Electric vehicles predominantly use liquid-cooled heatsinks for their traction inverter and rectifier modules. For example, the 2015 Tesla Model-S 70D features 36 paralleled TO-247 discrete packaged IGBTs enclosed within an internal cavity heat sink^{5,6}. Likewise, the Chevrolet Volt, Toyota Prius, and Nissan Leaf employ liquid-cooled heat sinks for their IGBT modules^{5,7-10}. Although liquid-cooled heat sinks are prevalent in EVs, their

integration mostly requires Thermal Interface Materials (TIM) for electrical isolation and to reduce contact thermal resistances. The impact of TIM on device thermal coupling has been discussed in refs. 11-13. In addition, liquid-cooled heat sinks are bulky and require substantial coolant volumes. For example, the inverter module on the Tesla Model S 2015 weighs 5.8 kg and has 6.4 liters of internal volume⁵. Furthermore, liquid-cooled heat sinks are positioned farther from the device thermal junctions, making conduction heat losses more significant than convection through the heat sink. An overview of trends and challenges in thermal management for power converters is provided in refs. 14-17.

In contrast, direct-to-chip (D2C) liquid cooling solutions based on micro-channel and micro-convection are gaining interest, particularly for data centers and high-performance computing applications¹⁸⁻²¹. A co-designed GaN-on-Silicon AC-DC converter with monolithically integrated microchannels on a passive silicon substrate was demonstrated in ref. 22,23. Likewise, TSMC developed a liquid cooling solution directly to silicon by embedding microchannels into a silicon lid²⁴. Chip-level integration minimizes the thermal gap and substantially reduces thermal resistances, while offering the benefits of high performance, low energy consumption, smaller footprint area, and reduced coolant volumes. Despite their benefits, direct-

¹Chip Integration Technology Center (CITC), Nijmegen, The Netherlands. ²Netherlands Organisation for Applied Scientific Research TNO, Den Haag, The Netherlands. ³Delft University of Technology, Delft, The Netherlands. ⁴Hochschule Rhein-Waal, Kleve, Germany. ⁵Nexperia BV, Nijmegen, The Netherlands.

e-mail: henry.martin@tno.nl

to-chip liquid cooling encounters integration complexities and scalability issues, as highlighted in ref. 25.

Hence, we introduce an alternative integration approach of co-packaging electronics with microfluidics that enables direct-to-package (D2P) cooling. In Table 2, a comparative summary listing the advantages and limitations of commercial heat sink cooling, D2C cooling, and the proposed D2P cooling technologies is provided. The benefits of integrating cooling at a package-level reduce integration complexities and favor scalability, while eliminating the need for complex TIM management as required in most traditional heat sinks. Figure 1 illustrates the design and prototype of the direct-to-package cooling concept demonstrated in this study. A quad-flat no-leads (QFN) surface mount package type was chosen due to ease of demonstration, which encloses a silicon chip sintered onto a copper substrate with embedded microchannels. In this paper, the heat dissipation capability of the D2P cooling approach was demonstrated

up to $\sim 625 \text{ W cm}^{-2}$ with a maximum coolant flow rate of 0.2 ml s^{-1} , and the maximum junction temperature capped at $300 \text{ }^\circ\text{C}$. Based on the experimental results, the following observations were drawn:

1. $\sim 6\text{--}7\times$ lower junction temperature and thermal resistance is achieved when compared to packages with ambient air convection cooling.
2. $\sim 2\text{--}3\times$ lower junction temperature and thermal resistance is achieved when compared to packages mounted on a liquid-cooled heat sink (30 ml s^{-1}) with TIM.
3. High Coefficient of Performance (COP) exceeding 10^3 at a ΔT of $60 \text{ }^\circ\text{C}$, and 10^4 at a ΔT of $275 \text{ }^\circ\text{C}$ is achieved, with very high effective Global Nusselt numbers ($\text{Nu}_{\text{eff-G}} > 10$), which is in par to D2C cooling methods.

The convective heat transfer of the proposed concept can be further improved by optimizing the microchannel topology and coolant parameters. Notably, the proposed D2P solution is not limited to single-phase fluids, but can facilitate phase transition with latent heat of evaporation to enhance heat absorption²⁶⁻²⁹.

Results

Performance analysis

To quantify the benefits of D2P cooling, two surface mount package configurations were realized:

- Reference packages with bulk copper substrate.
- Microfluidic packages with micro-channel integrated copper substrate.

Table 1 | Typical values of convective heat transfer coefficient h of different fluids³², and their corresponding heat flux Q limits determined for a ΔT of $275 \text{ }^\circ\text{C}$

Medium	$h \text{ W m}^{-2} \text{ K}^{-1}$	$Q \text{ W cm}^{-2}$
Free convection - Gases; Liquids	2–25; 50–1000	0.06–0.69; 1.38–27.5
Forced convection - Gases; Liquids	25–250; 100–20000	0.69–6.88; 2.75–550.0
Convection with phase change boiling or condensation	2500–100,000	68.75–2750.0

Table 2 | Comparison of cooling technologies: Heat Sink, Direct-to-Chip, and Direct-to-Package

	Heat Sink Cooling (Current Commercial Technology)	Direct-to-Chip (D2C) Cooling (State-of-the-Art Technology)	Direct-to-Package (D2P) Cooling (Proposed Technology)
Integration Method	Integrated (mostly) using TIM	Integrated within the semiconductor substrate	Integrated within the package substrate
Thermal Network	Chip → Die-Attach → Package Substrate → TIM → Liquid-cooled Heat Sink	Chip → Liquid-cooled Semiconductor Substrate	Chip → Die-Attach → Liquid-cooled Package Substrate
Advantages	<ol style="list-style-type: none"> 1. Size and geometry similar to traditional heat exchangers. 2. Multiple devices can be cooled. 3. Easy to manufacture and scale. 4. Low integration complexity. 5. High mechanical robustness. 6. No electrical isolation concerns. 	<ol style="list-style-type: none"> 1. Substantially lower thermal resistance. 2. Enables maximum device performance. 3. Lowers energy consumption. 4. Very small footprint area. 5. Less coolant consumption. 	<ol style="list-style-type: none"> 1. Low thermal resistance. 2. Comparable performance to direct-to-chip cooling. 3. Lowers energy consumption. 4. Small footprint area. 5. Less coolant consumption. 6. Low integration complexity. 7. Feasible on lateral and vertical transistors (needs electrical isolation). 8. Easy to manufacture and scale. 9. Supports heterogeneous integration (chiplets, multi-chip packages). 10. Thermo-mechanical stresses better managed.
Limitations	<ol style="list-style-type: none"> 1. Relatively high thermal resistance (poor TIM conductivity). 2. Complexity in TIM management. 3. Limits maximum device performance. 4. High energy consumption. 5. Requires large footprint. 6. Large coolant volumes needed. 7. Poor scalability with increasing power density. 	<ol style="list-style-type: none"> 1. Very high integration complexity (wafer-level fabrication and a thick passive semiconductor). 2. Not suitable for vertical transistors. 3. Hard to commercialize at scale. 4. Devices must be individually cooled. 5. Maintenance challenges. 	<ol style="list-style-type: none"> 1. Devices must be individually cooled. 2. Maintenance challenges.
Application	Mid-to-high power electronics	High-power, high-density (AI accelerators)	Mid-to-high power, chiplets, multi-chip packages

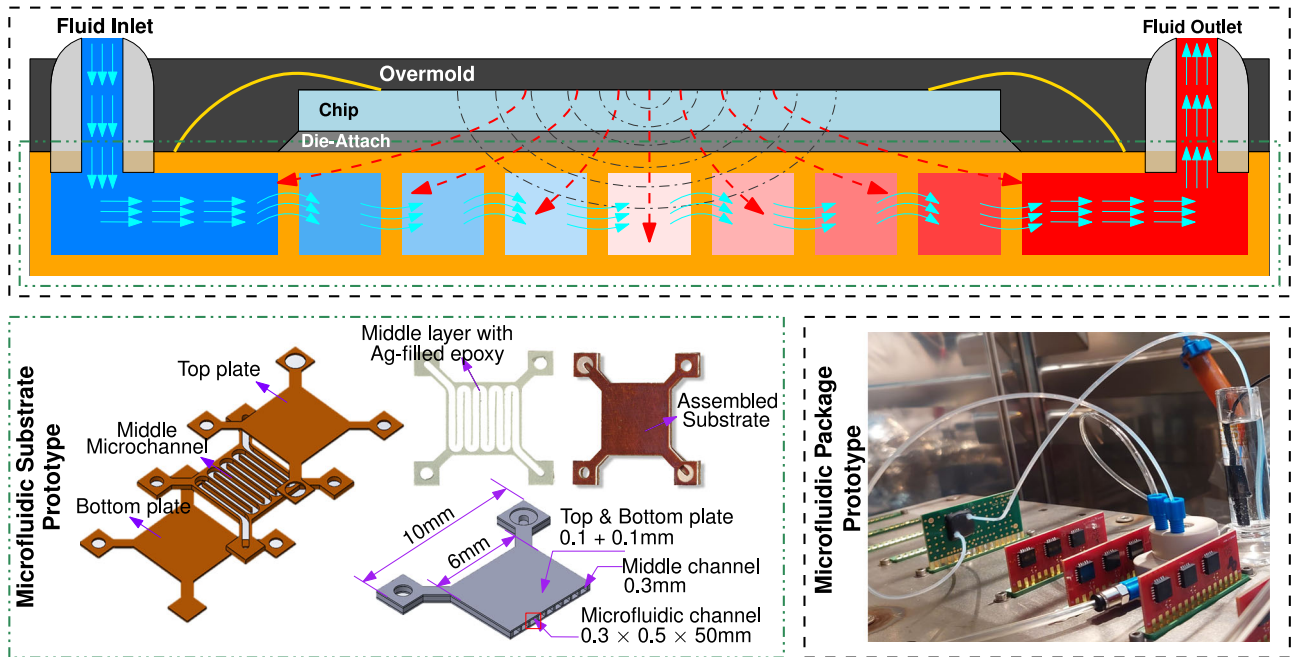


Fig. 1 | Design and prototype of the direct-to-package cooling concept. A schematic illustration of the proposed concept is shown at the top, and the assembly of the microfluidic substrate and package prototype is shown at the bottom.

In this study, Thermal Test Chips (TTCs) with integrated heaters and temperature sensors were used as an active device. Calibration of both heaters and temperature sensors is explained under the methods section. It is important to note that the heating elements cover ~62% of the total chip area. Hence, the heat flux needs to be computed based on the area of the heating elements. The reference packages with bulk copper substrate were tested as follows:

- Reference packages on PCB with ambient air convection cooling, and
- Reference packages on PCB with forced convection cooling using a liquid-cooled heat sink.

The thermal vias on the PCB transfer the heat from the package to the heat sink through the thermal interface material (TIM). The results of the reference packages were further compared to microfluidic packages tested at 0.1 ml s^{-1} , 0.15 ml s^{-1} , and 0.2 ml s^{-1} (see Fig. 2a).

An input power of 2.64 W (Current $I = \text{constant}$) was applied onto the heaters that are distributed over the TTC surface, and the junction temperature (T_j) was measured using the temperature sensor until thermal equilibrium (steady-state) was reached. Due to the increasing surface temperature, the electrical resistance of the heaters also increases, resulting in higher input power as the device reaches steady-state conditions. The temperature sensitivity of the heaters was determined to be $\sim 0.047 \text{ } \Omega \text{ } ^\circ\text{C}^{-1}$, which is explained under the methods section. Accordingly, the resulting power input P_{in} at steady-state was determined for all test case conditions, i.e., for reference packages with and without a heat sink, and also for microfluidic packages at different flow rates (see Fig. 2a)

The reference packages with ambient convection cooling reached a steady-state T_j of $\sim 220^\circ\text{C}$ over 1000 seconds with P_{in} increasing from 2.64 W to 4.11 W (see Fig. 2a). Likewise, the reference packages mounted onto a heat-sink reached a steady state T_j of $\sim 78^\circ\text{C}$ over 100 s with P_{in} increasing from 2.64 W to 3.05 W, and consumed three liters of coolant flowing at a constant rate of 30 ml s^{-1} . In contrast, the microfluidic packages attained a steady-state T_j of $\sim 43^\circ\text{C}$ in under 20 s with P_{in} increasing from 2.64 W to 2.78 W (see Fig. 2a). The microfluidic packages were tested at different flow rates, 0.1 ml s^{-1} , 0.15 ml s^{-1} , and 0.2 ml s^{-1} , with a maximum coolant volume of less than four milliliters to reach a steady-state T_j . The transient response of the microfluidic

packages indicates a shift in time scale due to lower thermal capacitance (less copper) than bulk copper substrates. Also, marginal variations in ΔT_j ($\pm 0.5^\circ\text{C}$) were observed at different flow rates, likely due to insufficient heating with the applied power input. The experiments were further repeated with varying power inputs (see Fig. 2b).

The maximum T_j was constrained to the solder reflow temperature of 300°C , thereby limiting a maximum ΔT of 275°C . A linear slope was fitted to the measurement results. With a heating power of less than 6 W at steady state conditions, the reference packages with ambient convection cooling reach a maximum steady-state ΔT of $\sim 275^\circ\text{C}$. Likewise, the reference packages with liquid-cooled heat sink reach a ΔT of $\sim 170^\circ\text{C}$ at $\sim 9 \text{ W}$, when further extrapolated to a ΔT of 275°C , indicates $\sim 14 \text{ W}$ input power. This highlights that with proper thermal management, the device’s power dissipation capability can be improved.

In case of microfluidic packages, the distance between the thermal junctions and the cooling components is significantly smaller, which enables to dissipate higher power over the same device footprint. At 0.1 ml s^{-1} , a ΔT of $\sim 275^\circ\text{C}$ was reached at $\sim 37 \text{ W}$, marking a $\sim 6\text{--}7 \times$ increase over the reference packages under ambient air convection and a $\sim 2\text{--}3 \times$ increase over the reference packages mounted onto a heat sink. At 0.15 ml s^{-1} and 0.2 ml s^{-1} , a ΔT of $\sim 275^\circ\text{C}$ corresponds to $\sim 38 \text{ W}$ and $\sim 41 \text{ W}$, respectively. The maximum input power at a ΔT of 275°C for all three cases is tabulated in Table 3. The corresponding heat flux Q at steady state, highlighted in Fig. 2b, was determined by dividing the heater power input at steady state by the heating element area.

It is important to realize that the choice of surface mount package configuration in this study necessitates a PCB between the package and the heat sink. However, this does not adequately represent the current commercial technology, where Through Hole (TO) packages come in direct contact with the heat sink. Hence, we addressed this discrepancy through thermal simulations (see Supplementary Fig. 4), where the reference packages mounted onto a heat sink are simulated with and without a PCB.

To further quantify the performance of direct-to-package cooling, the Coefficient of Performance (COP) parameter was determined. In ref.²², the COP is defined as the ratio of extracted power to the pumping power while maintaining a steady-state temperature difference ΔT_{max} of 60°C as

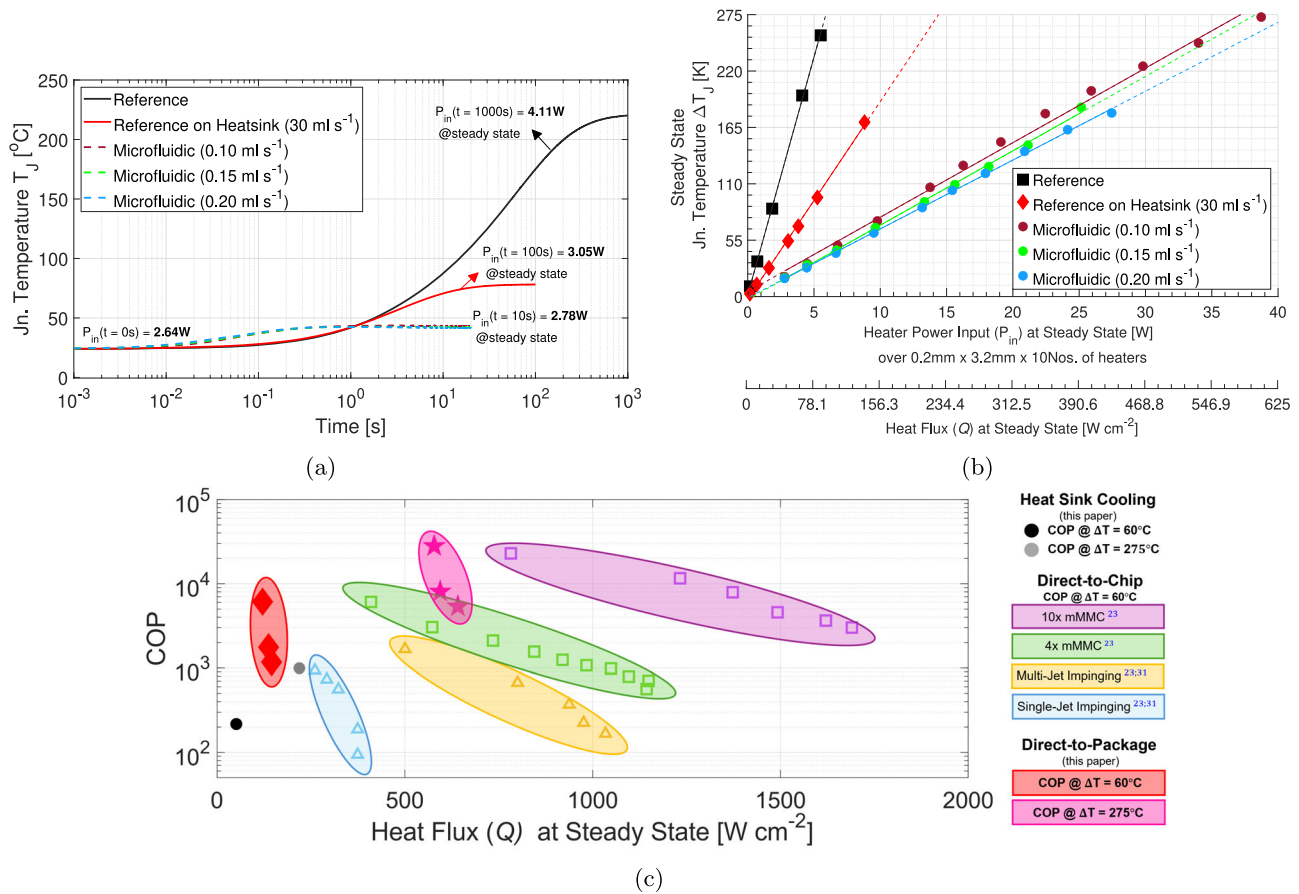


Fig. 2 | Overview of thermal performance characterization and comparison across different cooling strategies. **a** Transient to steady-state thermal measurements comparing the reference package (with ambient cooling and heat sink cooling—30 ml s⁻¹), and the microfluidic-cooled package at 0.1 ml s⁻¹, 0.15 ml s⁻¹, and 0.2 ml s⁻¹ flow rates. **b** Steady-state junction temperature variation as a function of power input and

heat flux in W cm⁻². A linear slope was fitted to the measurements. **c** Coefficient of Performance (COP) plotted against heat flux for different cooling technologies. COP values are based on steady-state ΔT of 60 °C and 275 °C. The COPs for monolithic manifold microchannels are experimental-based at ΔT of 60 °C reported in ref. 22, while jet-impingement results are simulation-based at ΔT of 60 °C reported in refs. 22,30.

Table 3 | Comparative summary of experimental results for all three test cases

	Reference ambient air convection	Reference on heatsink 30 ml s ⁻¹	Microfluidic package		
			0.1 ml s ⁻¹	0.15 ml s ⁻¹	0.2 ml s ⁻¹
Max. P_{in} [W] @ $T_j = 300^\circ C$	6	14	37	38	41
R_{total} [K W ⁻¹]	46.42	19.30	7.27	7.25	6.72
$R_{caloric-eff}$ [K W ⁻¹]	–	–	1.15	1.09	0.87
$R_{conv-eff}$ [K W ⁻¹]	–	–	5.80	5.84	5.53
R_{cond} [K W ⁻¹]	–	–	0.32	0.32	0.32
h_{eff-G} [W m ⁻² K ⁻¹]	–	–	16844	16722	17672
NU_{eff-G} [–]	–	–	10.41	10.34	10.93
Coolant volume [ml]	–	3000	2	3	4

expressed in Equation (1),

$$COP = \frac{\Delta T_{max}}{P_{pump} R_{total}} \quad (1)$$

where P_{pump} is the pumping power ($P_{pump} = f\Delta P$), which is the product of the volumetric flow rate f and the pressure drop ΔP (see Supplementary Fig. 2), and R_{total} is the total thermal resistance (junction-to-ambient). The R_{total} can be determined from Eq. (2),

which corresponds to the slope of the linear line fitted in Fig. 2b.

$$R_{total} = \frac{\Delta T_j}{\Delta P_{in}} \quad (2)$$

Accordingly, the COP was determined at a ΔT_{max} of 60 °C and 275 °C for both reference packages on heat sink cooling and the microfluidic packages (see Fig. 2c). The coefficient of performance (COP) at a ΔT of 275 °C is representative of transistors operating at higher temperatures. For

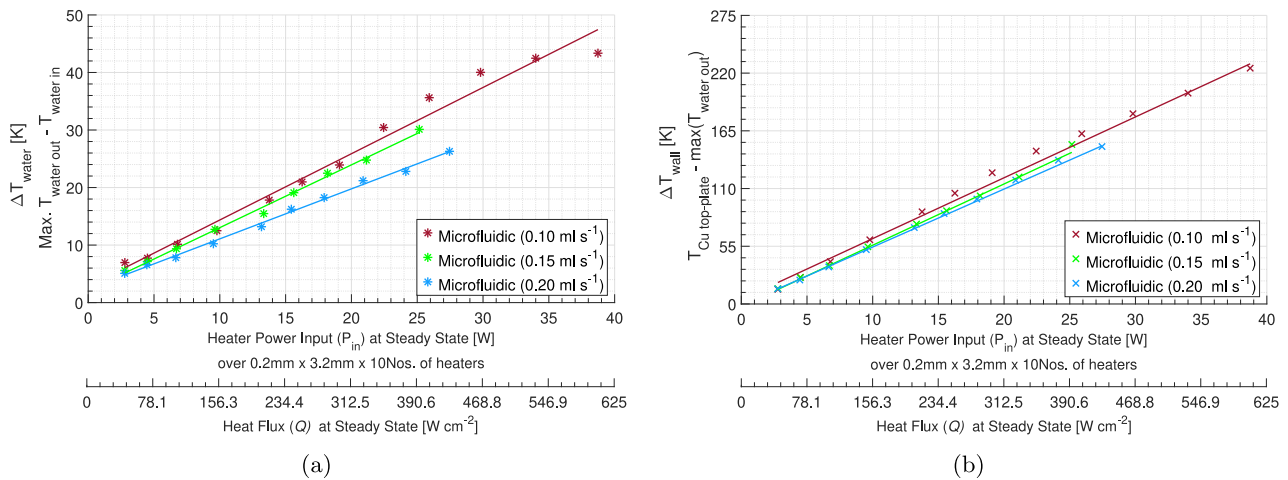


Fig. 3 | Temperature variations across the microfluidic cooling system under different power inputs. a Variation in coolant (water) temperature and **b** Variation in wall temperature as a function of power input and heat flux. A linear relationship was established in each plot (a, b).

comparative analysis, the COP of direct-to-chip (D2C) cooling is shown for both monolithically integrated manifold microchannel ($4 \times$ and $10 \times$ integration density) demonstrated in ref.²², and the jet-impinging cooling technology simulated in ref.³⁰. A relatively high COP exceeding 10^3 at a ΔT of 60°C , and 10^4 at a ΔT of 275°C , was observed with direct-to-package (D2P) cooling, which is in par with the direct-to-chip (D2C) cooling technology at the lower heat flux range.

Heat transport efficiency analysis

The R_{total} of the microfluidic packages indicates the lowest system resistance as compared to reference packages. For microfluidic packages, the R_{total} is the summation of caloric thermal resistance R_{caloric} , convective thermal resistance R_{conv} , and conductive thermal resistance R_{cond} .

$$R_{\text{total}} = R_{\text{caloric}} + R_{\text{conv}} + R_{\text{cond}} \quad (3)$$

In principle, R_{caloric} can be determined based on the change in coolant temperature ($\Delta T_{\text{water}} = T_{\text{water out}} - T_{\text{water in}}$) and the power dissipated through the coolant ($P_{\text{coolant}} = \dot{m} c_p \Delta T_{\text{water}}$), where ρ and c_p are the coolant properties. While the inlet water temperature is in a steady state, the outlet temperature exhibits a transient behavior, though the device junction has reached a thermal equilibrium. Ideally, the local temperature of the coolant directly beneath the chip needs to be recorded. In practice, this temperature cannot be measured directly; therefore, the maximum outlet temperature of the coolant recorded using a thermocouple was used as an approximation to determine ΔT_{water} (see Fig. 3a). Consequently, the fraction of power dissipating through the coolant (P_{coolant}) is unknown. Hence, an effective caloric resistance $R_{\text{caloric-eff}}$ was determined from Equation (4), where the applied input power ΔP_{in} was considered, which corresponds to the slope of the line fitted in Fig. 3a. The derived $R_{\text{caloric-eff}}$ is provided in Table 3.

$$R_{\text{caloric-eff}} = \frac{\Delta T_{\text{water}}}{\Delta P_{\text{in}}} \quad (4)$$

Likewise, to determine the convective thermal resistance R_{conv} , the wall temperature ΔT_{wall} must be obtained, i.e., the temperature difference between the top copper plate of the microfluidic channel (T_{Cu}) and the coolant. To determine T_{Cu} , a one-dimensional heat transfer model was assumed, which also accounts for the lateral heat spreading resistance within the top plate (see Supplementary Fig. 1). It is important to note that the coolant temperature relevant to ΔT_{wall} should ideally correspond to the local bulk temperature of the coolant near the wall surface, since there are thermal losses along the ferrules and outlet tubing. Consequently, the recorded maximum outlet temperature is an underestimation of the actual coolant

temperature near the wall surface. However, the maximum outlet coolant temperature is expected to be a more realistic estimate to determine ΔT_{wall} than the mean coolant temperature between the inlet and outlet. Furthermore, the P_{coolant} is not known. Hence, an effective convection resistance $R_{\text{conv-eff}}$ based on ΔP_{in} was derived from Equation (5), which corresponds to the slope of the linear line in Fig. 3b. The derived $R_{\text{conv-eff}}$ is provided in Table 3.

$$R_{\text{conv-eff}} = \frac{\Delta T_{\text{wall}}}{\Delta P_{\text{in}}} \quad (5)$$

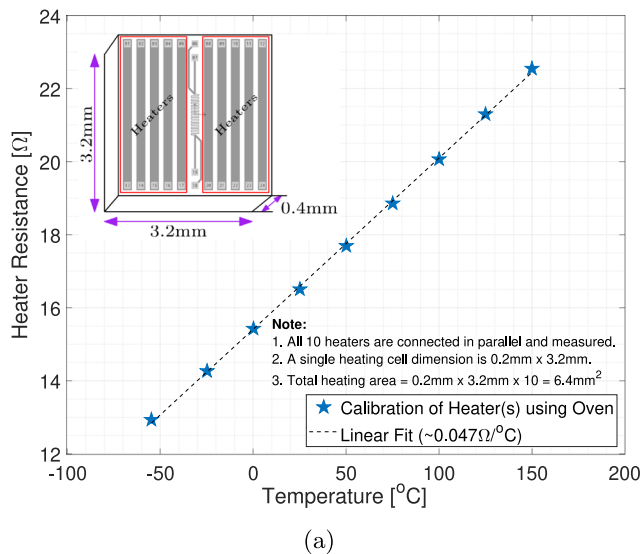
It is important to note that only $\sim 78\%$ of the total chip area ($A_{\text{chip}} = 3.2 \text{ mm} \times 3.2 \text{ mm}$) is in direct contact with the coolant, i.e., the wetted area = $\sim 78\%$ of A_{chip} , and the remaining $\sim 22\%$ is bonded via a silver-filled epoxy adhesive. As a result, the $R_{\text{conv-eff}}$ parameter represents an effective thermal resistance from the top copper plate to the fluid outlet. The obtained $R_{\text{conv-eff}}$ accounts for the convective heat transfer through the coolant-contacted region, the conductive heat transfer through the epoxy-bonded region, and the lateral heat spreading resistance on the top copper plate. Consequently, $R_{\text{conv-eff}}$ includes parallel thermal paths and should not be interpreted as a pure convective resistance. The obtained $R_{\text{conv-eff}}$ shows relatively less dependence on the flow rate as compared to $R_{\text{caloric-eff}}$ (see Table 3).

Subsequently, R_{cond} can be determined from Eq. (3), where the effective caloric and convective resistances are considered. The obtained R_{cond} includes the conductive resistance contribution from the die to the top copper plate predominantly, and it remains independent of the fluidic flow rates. A summary of thermal resistances is provided in Table 3. It is explicit that the $R_{\text{conv-eff}}$ is higher than $R_{\text{caloric-eff}}$ and R_{cond} due to additional components such as heat spreading resistance and conductive resistance through the epoxy-bonded region. However, optimizing the microfluidic design and the coolant parameters will facilitate reducing the convective resistances.

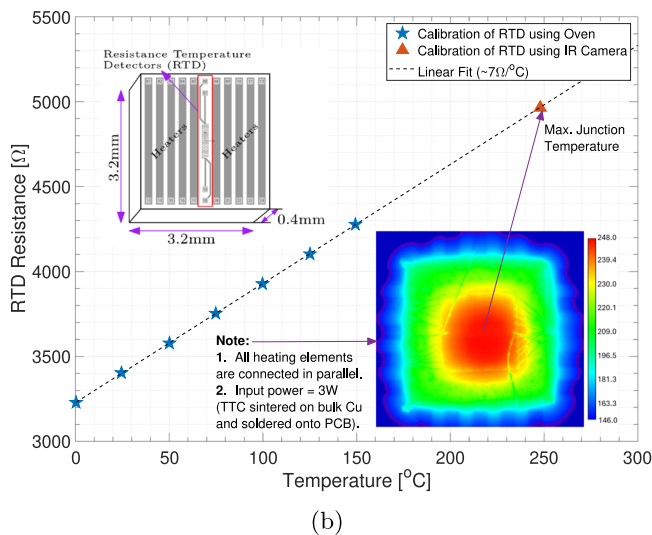
Furthermore, the effective global heat transfer coefficient $h_{\text{eff-G}}$ was obtained from the experimentally determined convective resistance $R_{\text{conv-eff}}$ and the total chip footprint area A_{chip} (see Eq. (6)).

$$h_{\text{eff-G}} = \frac{1}{R_{\text{conv-eff}} \cdot A_{\text{chip}}} \quad (6)$$

Since $R_{\text{conv-eff}}$ was determined based on a one-dimensional model (see Supplementary Fig. 1), the extracted $h_{\text{eff-G}}$ is a lumped (area-averaged) heat transfer coefficient referenced to the total chip area A_{chip} . To further evaluate the heat-transfer performance, an effective global Nusselt number ($Nu_{\text{eff-G}}$)



(a)



(b)

Fig. 4 | Calibration of heating elements and Resistance-based Temperature Detector (RTD). **a** The resistance of all parallelly connected heaters was measured at nine different temperatures between $-55\text{ }^{\circ}\text{C}$ and $+150\text{ }^{\circ}\text{C}$. **b** The RTD resistance was measured at seven different temperatures between $0\text{ }^{\circ}\text{C}$ and $+150\text{ }^{\circ}\text{C}$. To determine the RTD sensitivity at higher temperatures, 3W power input was applied to the heaters, while the steady state temperature was recorded using an IR camera, and the RTD resistance was simultaneously measured. Both plots (a) and (b) exhibit a linear relation.

was calculated using Eq. (7).

$$Nu_{\text{eff-G}} = \frac{h_{\text{eff-G}} \cdot D_H}{k_f} \quad (7)$$

where D_H is the hydraulic diameter of the microchannel, and k_f is the thermal conductivity of the coolant (for water $k_f = 0.6065\text{ W m}^{-1}\text{ K}^{-1}$). Accordingly, a $Nu_{\text{eff-G}} > 10$ was obtained, indicating very high dissipation capability of the microfluidic packages. $Nu_{\text{eff-G}}$ determined in Eq. (7) yields an overall, dimensionless measure of the device’s thermal performance representing the system-level heat transfer. The obtained $h_{\text{eff-G}}$ and $Nu_{\text{eff-G}}$ is reported in Table 3.

Despite relatively higher $R_{\text{conv-eff}}$, the effective heat transfer performance, denoted as $Nu_{\text{eff-G}}$, of the microfluidic integrated system indicates very high dissipation capability, which must be due to the convective heat transfer through the coolant integrated closer to the device thermal junction. Optimizing the micro-channel substrate design and the coolant parameters

can further improve the heat transport efficiency of the microfluidic packages. Erp. et. al.,²² reports Nusselt numbers for microchannels integrated on semiconductor substrates, which range from 2.6 to 6 for straight parallel microchannels and a maximum of 16 for monolithic manifold microchannels. Though the localized convection-based Nusselt number was not determined in this study, the effective global Nusselt numbers demonstrated are in a comparable range to direct-to-chip cooling methods reported in ref. 22.

Discussion

In this study, a co-packaging approach was introduced for Direct-to-Package (D2P) cooling solution. This is particularly important as commercial solutions rely on bulky heat sinks with Thermal Interface Materials (TIM) and substantial coolant volumes to yield optimal thermal performance. Recent state-of-the-art developments focus on chip-level integration by either embedding micro-channels onto semiconductor substrates or micro-convection through jet-impingement. Despite the performance advantages of Direct-to-chip (D2C) cooling solution, they are complex, significantly expensive, and require a thick passive semiconductor substrate (for embedding micro-channels).

In contrast, our proposed D2P approach integrates micro-cooling channels onto the package substrate, thereby providing comparable thermal performance to D2C techniques, without the associated complexities. In this paper, a significant reduction in total thermal resistance was demonstrated with D2P cooling, leading to a lower steady-state junction temperature compared to ambient air cooling and liquid-cooled heat sinks. Notably, the proposed solution consumed a fraction of the coolant volume required by traditional heat sinks. The Coefficient of Performance (COP) exceeded 10^3 at a ΔT of $60\text{ }^{\circ}\text{C}$, and 10^4 at a ΔT of $275\text{ }^{\circ}\text{C}$ with a relatively high effective global Nusselt number comparable to D2C techniques.

- Design optimization and material compatibility: While this work validates the feasibility of D2P cooling solution, future research should explore optimization strategies for channel geometry, fluidic flow, fabrication methods, and other dielectric fluids that are corrosion resistant.
- Alternative coolants and two-phase systems: Additional performance gains can be achieved by exploring different coolants, such as nanofluids, phase change materials, and phase transition fluids that use the latent heat of evaporation for heat absorption. However, two-phase systems require heat exchangers and condensers. Implementation of phase-change materials can potentially act as a thermal buffer.
- Scalability and packaging integration: A key future focus should be on integrating the D2P concept into standard packaging, especially in high-volume or automotive-grade systems. This includes ensuring mechanical reliability, manufacturability, and compatibility with assembly processes.
- Applicability to different transistor architectures: The D2P cooling strategy is not limited to lateral transistors. It can potentially be extended to vertical power devices as well, provided proper electrical insulation of the coolant needs to be ensured to mitigate parasitic leakage paths or shorting risks for both lateral and vertical transistors.
- Reliability and long-term operation: The microfluidic structures are subjected to thermal and mechanical stresses. Hence, it is important to assess the long-term reliability and pressure stability of the system.

The demonstrated co-packaged architecture for D2P cooling holds immense potential in realizing high-power electronic systems. Bridging the thermal gap by integrating cooling components closer to the device junction is broadly applicable across a wide range of applications, namely sustaining high power operation in SiC devices to enhancing RF power added efficiency in GaN amplifiers. Thus, the D2P cooling strategy can contribute to the development of reliable and sustainable electronics.

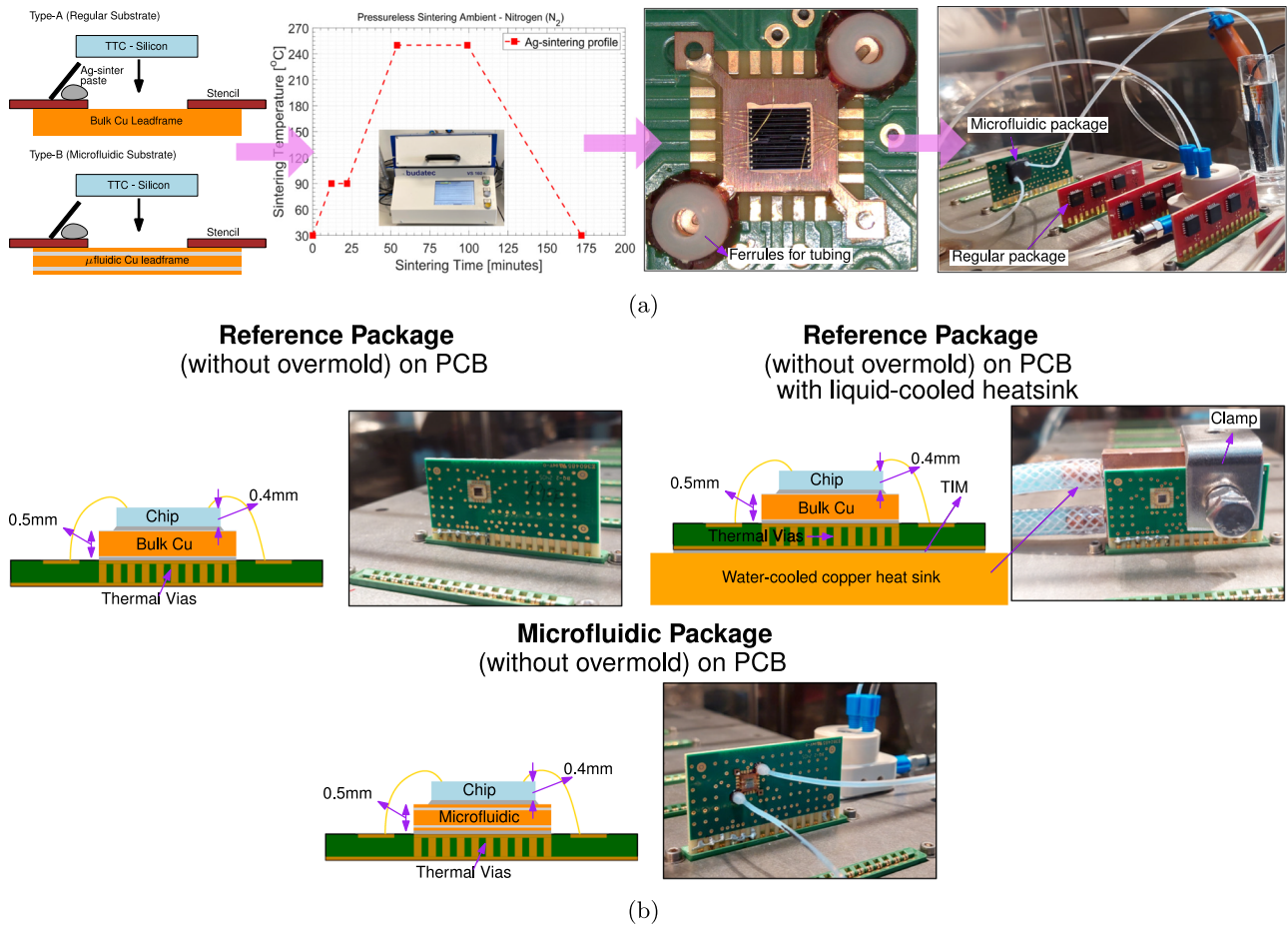


Fig. 5 | Overview of packaging assembly processes and experimental configurations for comparative thermal testing. a Step-by-step illustration of the package assembly process. **b** Visualization of different test cases featuring reference package

configuration and microfluidic package. For the reference package with a liquid-cooled heat sink, two clamps were used to ensure uniform compression; using a single clamp may result in uneven force distribution, leading to tilting or lift-off.

Methods

Selection and calibration of the semiconductor device

The choice of semiconductor device is crucial as it influences the package thermal performance analysis. Thermal Test Chips (TTC) are specialized devices fabricated through processes similar to semiconductor devices. The design of TTCs is intended to simulate device junction (surface) heating through lithographically defined heating elements, and the junction temperature is recorded using Resistance-based Temperature Detectors (RTDs). Hence, a commercial silicon-based TTC was used in this study (see Fig. 4).

The heating elements on TTC were connected in parallel to achieve a uniform temperature distribution along the surface. The RTD is located centrally with 4-point Kelvin contacts. It is essential to determine the temperature sensitivity of the heating elements and the RTD. In Fig. 4a, the resistance of the parallelly connected heating elements was measured at nine different temperatures from $-55\text{ }^{\circ}\text{C}$ to $150\text{ }^{\circ}\text{C}$. A perfectly linear relationship was determined with a sensitivity of $0.047\text{ }\Omega^{\circ}\text{C}^{-1}$. Likewise, the temperature sensitivity of the RTD was determined through a two-step calibration process. For calibration below $150\text{ }^{\circ}\text{C}$, the RTD was measured inside an oven at different ambient temperatures. For temperatures above $150\text{ }^{\circ}\text{C}$, an input power of 3 W was applied to the heaters by connecting all heating elements in parallel, and the change in RTD resistance was measured while simultaneously measuring the device junction temperature using an Infra-Red (IR) camera.

The measured RTD resistance and the junction temperature were in a steady state. A linear relationship was established by fitting both calibration measurements, resulting in a sensitivity of $\sim 7\text{ }\Omega^{\circ}\text{C}^{-1}$ (see Fig. 4b). For IR

measurements, the TTC was sintered on a bulk copper substrate, which was further soldered onto a PCB and wire bonded. The backside of the TTC (Silicon substrate) is metalized with TiPtAu ($100/100/100\text{ nm}$) to promote adhesion to the die-attach interface material.

Design and fabrication of microfluidic substrate

The design of the microchannel was chosen based on fabrication feasibility. A three-layered copper substrate with top and bottom copper plates was designed to enclose a serpentine-structured microchannel middle layer. The serpentine-channel design was realized through a laser-cut process. While optimizing the microchannel geometry is beyond the scope of this study, the serpentine configuration is expected to induce localized turbulence and enhance heat dissipation compared to straight microchannels. The serpentine microchannels have a dimension of $0.3\text{ mm} \times 0.5\text{ mm}$ with a total channel length of $\sim 50\text{ mm}$ between the inlet and outlet. The top and the bottom copper plates with 0.1 mm thickness each were attached to the microchannel middle layer using conductive Ag-filled epoxy adhesive. The coolant inlet and outlet were placed diagonally along the substrate through the top plate, with alignment markers positioned along the counter-diagonal. All details relevant to the embedded microchannel substrate are provided in Fig. 1.

Though the design optimization was not investigated in this study, we suggest the following improvements to be considered in the future. Simplifying the three-layered substrate into a two-layered substrate with half-etched microchannels bonded using thermal compression can be a scalable and efficient approach. Furthermore, coolant delivery in real-life applications could be implemented through PCBs.

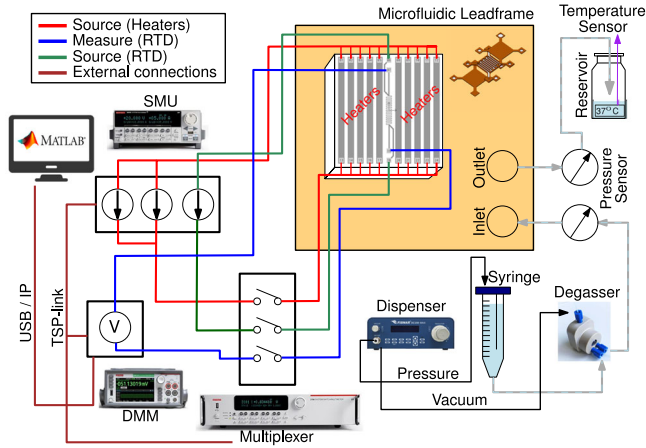


Fig. 6 | Schematic electrical and microfluidic circuit illustration.

Package assembly processes

The devices were assembled using classical back-end packaging processes, which involve three primary steps: Die-bonding, Wire-bonding, and Encapsulation. The selected TTCs were bonded onto the substrate using Ag-sinter die-attach material. Ag-paste in wet form was stencil-printed on the microfluidic substrate. The TTCs were placed over the wet paste using a force-controlled die-bonder and sintered pressureless under Nitrogen ambient at 250 °C. Ag-sintering material was chosen because of low processing temperatures and a high melting point after sintering. The die-bonding process is identical for reference samples with a bulk copper substrate. Upon sintering, the complete stack is soldered onto a printed circuit board (PCB) and subsequently wire-bonded onto the bond pads of the PCB using 99.99% pure Au-wire bonds. For microfluidic packages, inlet and outlet ferrules were securely placed using an adhesive. Finally, the assembled devices can be optionally encapsulated using a dam and fill encapsulant.

In this study, the devices were not encapsulated since the glass transition temperature of the encapsulant is less than the desired testing temperatures. An illustration of the package assembly processes is provided in Fig. 5a. In Fig. 5b, the two package configurations with different test cases are provided for experimental evaluation. In case of reference packages mounted onto a liquid-cooled heat sink, a silicone-free heat sink compound from Techspray was used as Thermal Interface Material (TIM), which has a conductivity of ~0.92 W/mK with functional temperature range of -40 °C to +200 °C. For heat sink cooling, the channel radius is 2 mm, and the estimated channel length is 10 cm.

Experimental setup for performance evaluation

To evaluate the package performance, a dedicated experimental setup was developed, as illustrated schematically in Fig. 6. Devices soldered to the PCB were securely mounted in a test socket, enabling electrical connections between the TTC and the measurement equipment via a multiplexer. The input currents for the heaters were sourced using a parallelly connected Source Measurement Unit (SMU) with compliance of 40 V up to 2 A continuous current. The change in RTD resistance was measured using a Digital MultiMeter (DMM), which has a resolution of 1 µV for measurements up to 10V and an accuracy of ± 0.1 mV. The SMU, DMM, and Multiplexer were synchronized through a Trigger Synchronization and Communication (TSP) protocol, and the measurement sequence was programmed using a user-defined MATLAB program. An open-loop microfluidic system was implemented to evaluate the cooling performance. A pressure dispenser with a maximum pressure of 675 kPa was connected to a 10 ml syringe carrying demineralized water as the coolant. Inlet coolant temperature was recorded, and the coolant was subsequently passed through a 300 µl degasser to remove air bubbles from the coolant, preventing blockage and localized explosions. The pressure difference before and after entering the microfluidic package was recorded using two pressure

sensors. The coolant outlet was collected in a reservoir, and the outlet temperature was measured with a thermocouple at one-millisecond intervals.

Data availability

This manuscript is part of the corresponding author’s (Henry A. Martin) Phd dissertation that is stored publicly as *Prognostics and thermal management of power electronic packages*. The experimental data that pertains to this manuscript are stored in the public repository <https://doi.org/10.6084/m9.figshare.31073227>.

Code availability

No custom code or mathematical algorithm that is deemed central to the conclusions has been developed for this manuscript.

Received: 11 April 2025; Accepted: 11 February 2026;

Published online: 25 March 2026

References

1. Yang, S. et al. An industry-based survey of reliability in power electronic converters. *IEEE Trans. Ind. Appl.* **47**, 1441–1451 (2011).
2. Joshi, S. N. et al. A review of select patented technologies for cooling of high heat flux power semiconductor devices. *IEEE Trans. Power Electron.* **38**, 6790–6794 (2023).
3. Wang, H., Liserre, M. & Blaabjerg, F. Toward reliable power electronics: challenges, design tools, and opportunities. *IEEE Ind. Electron. Mag.* **7**, 17–26 (2013).
4. Dhumal, A., Kulkarni, A. & Ambhore, N. A comprehensive review on thermal management of electronic devices. *J. Eng. Appl. Sci.* **70**, 140 (2023).
5. Reimers, J., Dorn-Gomba, L., Mak, C. & Emadi, A. Automotive traction inverters: current status and future trends. *IEEE Trans. Vehicular Technol.* **68**, 3337–3350 (2019).
6. R. J. Ramm, W. L. & Campbell, C. Heatsink with internal cavity for liquid cooling,” (2014).
7. Anwar, M., Hayes, M., Tata, A., Teimorzadeh, M. & Achatz, T. Power dense and robust traction power inverter for the second-generation Chevrolet Volt extended-range ev. *SAE International Journal of Alternative Powertrains* **4** (2015).
8. Anwar, M., Hasan, S. N., Teimor, M., Korich, M. & Hayes, M. B. Development of a power dense and environmentally robust traction power inverter for the second-generation Chevrolet Volt extended-range EV. In *2015 IEEE Energy Conversion Congress and Exposition (ECCE)*, 6006–6013 (2015).
9. Kitazawa, O. et al. Development of power control unit for compact-class vehicle. *SAE Int. J. Altern. Powertrains* **5**, 278–285 (2016).
10. Moreno, G., Bennion, K., King, C. & Narumanchi, S. Evaluation of performance and opportunities for improvements in automotive power electronics systems. In *2016 15th IEEE Intersociety Conference on Thermal and Thermomechanical Phenomena in Electronic Systems (ITherm)*, 185–192 (2016).
11. Li, X. et al. Impact of thermal interface materials on the device thermal coupling in semiconductor power modules. *IEEE Trans. Power Electron.* **40**, 3129–3137 (2025).
12. Heimler, P., Günther, M., Künzel, C., Lutz, J. & Basler, T. Influence of thermal interface material using discrete Si-IGBTs and consideration of power cycling conditions. *Microelectron. Reliab.* **150**, 115089 (2023).
13. Schulz, M., Allen, S. T. & Pohl, W. The crucial influence of thermal interface material in power electronic design. In *29th IEEE Semiconductor Thermal Measurement and Management Symposium*, 251–254 (2013).
14. Rahman, S. M. I. et al. Emerging trends and challenges in thermal management of power electronic converters: a state of the art review. *IEEE Access* **12**, 50633–50672 (2024).

15. Abramushkina, E., Zhaksylyk, A., Geury, T., El Baghdadi, M. & Hegazy, O. A thorough review of cooling concepts and thermal management techniques for automotive wbg inverters: Topology, technology and integration level. *Energies* **14** <https://www.mdpi.com/1996-1073/14/16/4981> (2021).
16. Garimella, S. V. et al. Thermal challenges in next-generation electronic systems. *IEEE Trans. Compon. Packag. Technol.* **31**, 801–815 (2008).
17. Dede, E. M. et al. Techno-economic feasibility analysis of an extreme heat flux micro-cooler. *iScience* **26**, 105812 (2023).
18. Zhang, H. & Guo, Z. Near-junction microfluidic cooling for gan hemt with capped diamond heat spreader. *Int. J. Heat. Mass Transf.* **186**, 122476 (2022).
19. Kearney, D., Hilt, T. & Pham, P. A liquid cooling solution for temperature redistribution in 3d ic architectures. *Microelectron. J.* **43**, 602–610 (2012).
20. Moloudi, R. et al. Metal-based direct multi-jet impingement cooling solution for autonomous driving high-performance vehicle computer (HPVC). In *2023 24th International Conference on Thermal, Mechanical and Multi-Physics Simulation and Experiments in Microelectronics and Microsystems (EuroSimE)*, 1–6 (2023).
21. Tiwei, T. et al. High efficiency direct liquid jet impingement cooling of high power devices using a 3D-shaped polymer cooler. In *2017 IEEE International Electron Devices Meeting (IEDM)*, 32.5.1–32.5.4 (2017).
22. Erp, R., Soleimanzadeh, R., Nela, L., Kampitsis, G. & Matioli, E. Co-designing electronics with microfluidics for more sustainable cooling. *Nature* **585**, 211–216 (2020).
23. Wei, T. All-in-one design integrates microfluidic cooling into electronic chips. *Nature* **585**, 188–189 (2020).
24. Wu, C. J. et al. Ultra high power cooling solution for 3D-ICS. In *2021 Symposium on VLSI Circuits*, 1–2 (2021).
25. Kong, R. et al. Enhancing data center cooling efficiency and ability: a comprehensive review of direct liquid cooling technologies. *Energy* **308**, 132846 (2024).
26. Shaeri, M. R., Bonner, R. W. & Ellis, M. C. Thin hybrid capillary two-phase cooling system. *Int. Commun. Heat. Mass Transf.* **112**, 104490 (2020).
27. Hasan, M. I. & Tbena, H. L. Using of phase change materials to enhance the thermal performance of micro channel heat sink. *Eng. Sci. Technol., Int. J.* **21**, 517–526 (2018).
28. Sohel Murshed, S. & Nieto de Castro, C. A critical review of traditional and emerging techniques and fluids for electronics cooling. *Renew. Sustain. Energy Rev.* **78**, 821–833 (2017).
29. Elshaer, A., Soliman, A., Kassab, M. & Hawwash, A. Boosting the thermal management performance of a PCM-based module using metallic pin fin geometries: numerical study. *Sci. Rep.* **13**, 10955 (2023).
30. Ndao, S., Peles, Y. & Jensen, M. Multi-objective thermal design optimization and comparative analysis of electronics cooling technologies. *Int. J. Heat. Mass Transf.* **52**, 4317–4326 (2009).
31. Ramires, M. L. V. et al. Standard reference data for the thermal conductivity of water. *J. Phys. Chem. Ref. Data* **24**, 1377–1381 (1995).
32. Incropera, F., DeWitt, D., Bergman, T. & Lavine, A. *Fundamentals of Heat and Mass Transfer* (2007).

Acknowledgements

This work has been made possible through the Dutch Growth Fund Programme POLARIS (Pathway towards Opportunities for Large scale Applications of Radically Integrated Systems). The POLARIS programme seeks to advance the state of the art RF systems and invests in Research &

Development as well as developing human capital and ecosystems. The authors gratefully acknowledge Berliner Nanotest and Design GmbH for the thermal test chip used in this work. The authors extend their gratitude to fellow researchers from the Delft University of Technology (TUD) and Chip Integration Technology Center (CITC) for their valuable support, particularly Frans Meeuwssen—Packaging Engineer at CITC, Jackson Gualberto de Sousa—Process Engineer at CITC, and Martien Kengen—Lab and Assembly Process Manager at CITC. Special thanks to John Janssen from NXP for supporting with the IR measurements for device calibration.

Author contributions

• Henry A. Martin: Conceptualization; Methodology; Validation; Formal analysis; Investigation; Resources; Data curation; Writing—Original Draft; Writing—Review and Editing; Visualization. • Zihan Zhang: Software (thermal simulations); Validation support. • Mahad Saeed: Investigation. • Sander Dorrestein: Conceptualization; Resources. • Edsger C. P. Smits: Conceptualization; Supervision; Project administration. • Rene H. Poelma: Conceptualization; Supervision. • Willem D. van Driel: Supervision. • GuoQi Zhang: Supervision.

Competing interests

The authors declare no competing interests.

Additional information

Supplementary information The online version contains supplementary material available at <https://doi.org/10.1038/s44172-026-00620-9>.

Correspondence and requests for materials should be addressed to Henry A. Martin.

Peer review information *Communications Engineering* thanks the anonymous reviewers for their contribution to the peer review of this work. Primary Handling Editors: [Philip Coatsworth]. A peer review file is available.

Reprints and permissions information is available at <http://www.nature.com/reprints>

Publisher's note Springer Nature remains neutral with regard to jurisdictional claims in published maps and institutional affiliations.

Open Access This article is licensed under a Creative Commons Attribution-NonCommercial-NoDerivatives 4.0 International License, which permits any non-commercial use, sharing, distribution and reproduction in any medium or format, as long as you give appropriate credit to the original author(s) and the source, provide a link to the Creative Commons licence, and indicate if you modified the licensed material. You do not have permission under this licence to share adapted material derived from this article or parts of it. The images or other third party material in this article are included in the article's Creative Commons licence, unless indicated otherwise in a credit line to the material. If material is not included in the article's Creative Commons licence and your intended use is not permitted by statutory regulation or exceeds the permitted use, you will need to obtain permission directly from the copyright holder. To view a copy of this licence, visit <http://creativecommons.org/licenses/by-nc-nd/4.0/>.

© The Author(s) 2026